

Identification of Burgers vectors of dislocations in monoclinic β -Ga₂O₃ via synchrotron X-ray topography

Yongzhao YAO^{1,*}, Yoshihiro SUGAWARA¹, Yukari ISHIKAWA¹, and Keiichi HIRANO²

¹ Japan Fine Ceramics Center,

2-4-1 Mutsuno, Atsuta, Nagoya, Aichi 456-8587, Japan

² Photon Factory, Institute of Materials Structure Science,

High Energy Research Organization,

1-1 Oho, Tsukuba, Ibaraki 305-0801, Japan

1 Introduction

Dislocations are major structural defects in semiconductor materials, and they have negative impacts on the performance and reliability of electronic devices. The Burgers vector (\vec{b}) of a dislocation is one of the most important characteristics that determines its behavior in an operating device. In this study, we used synchrotron X-ray topography (XRT) to perform systematic observations of dislocations in β -Ga₂O₃, which is a promising wide-bandgap semiconductor for power device applications. By applying the $\vec{g} \cdot \vec{b}$ invisibility criterion to dislocation contrasts in XRTs taken at multiple reciprocal lattice vectors \vec{g} , we identified 12 types of Burgers vectors, including 11 types theoretically predicted in the literature [1] and $\vec{b} = \langle 100 \rangle$. Some of these Burgers vectors, such as $\vec{b} = \langle 10\bar{1} \rangle$, $\frac{1}{2}\langle 132 \rangle$, $\frac{1}{2}\langle 1\bar{3}2 \rangle$, $\langle 001 \rangle$, and $\langle 100 \rangle$, were confirmed experimentally for the first time [2]. This report is based on the data published in ref. [2].

2 Experiment

The sample used in this work was a commercial single-crystal substrate with a $(\bar{2}01)$ -oriented surface. Synchrotron monochromatic-beam XRT was acquired at beamlines BL-3C and BL-14B (KEK-PF). Fig.1 shows a schematic of the experimental setups.

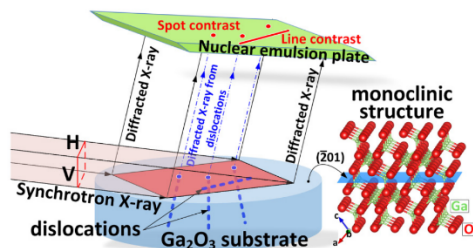


Fig. 1: Schematic of the experimental setup [2].

Grazing-incidence reflection geometry (Bragg case) was used with X-ray incident angles of about 5° with respect to the sample surface in most cases except for that of symmetric diffraction (e.g., $\vec{g} = \bar{6}03$ and $\vec{g} = \bar{1}206$), where large incident angles must be used for image recording. The wavelength of the X-ray was adjusted within the range of $0.836 \text{ \AA} - 2.314 \text{ \AA}$, in accordance with the selected \vec{g} and the incident angle. XRT images of the same sample area

were obtained at different \vec{g} vectors in order to determine the Burgers vectors of dislocations via the $\vec{g} \cdot \vec{b}$ invisibility criterion. Topographic images were recorded on $25.4 \text{ mm} \times 76.2 \text{ mm}$ nuclear emulsion plates, set at a distance of $10 \text{ cm} - 25 \text{ cm}$ from the sample with their surfaces perpendicular to the diffracted X-ray.

3 Results and Discussion

24 types of \vec{g} -vectors were employed. A list of these \vec{g} -vectors and the dislocation contrast with various Burgers vectors recorded using these \vec{g} -vectors can be found in ref. [2]. One of the most important types of dislocation, in terms of its density and its role in power devices, is the b -axis screw type dislocation with $\vec{b} = \langle 010 \rangle$.

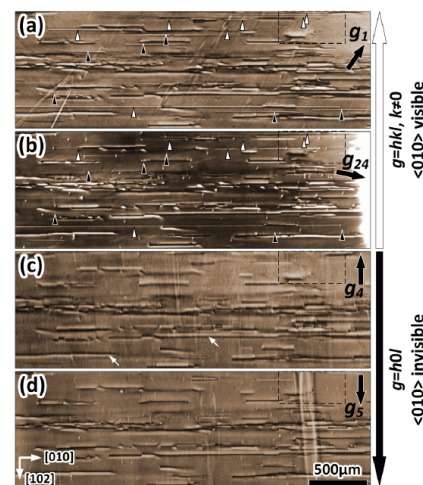


Fig. 2: XRT images used to identify the Burgers vector $\vec{b} = \langle 010 \rangle_{\text{screw}}$, taken at (a) $\vec{g}_1 = \bar{1}112$, (b) $\vec{g}_{24} = \bar{5}13$, (c) $\vec{g}_4 = \bar{1}200$, and (d) $\vec{g}_5 = 006$ [2].

Fig.2(a)–(d) show XRT images of the same sample area taken at 4 different \vec{g} vectors [2]. First, we consider the thin, line-shaped contrasts that extend horizontally in the $\langle 010 \rangle$ direction. These are indicated by white and black triangular marks. These lines are out of contrast at $\vec{g}_4 = \bar{1}200$ and $\vec{g}_5 = 006$, which indicates that they correspond to dislocations with a Burgers vector $\vec{b} // (\vec{g}_4 \times \vec{g}_5)$, i.e., $\vec{b} // \langle 010 \rangle$. Since they have a relationship of $\vec{b} // \vec{\zeta} // \langle 010 \rangle$, they are assigned to b -axis screw-type

dislocations. Some of these dislocations have a $\langle 010 \rangle$ length greater than 3 mm, which suggests that screw-type dislocations along the growth direction are stable during EFG.

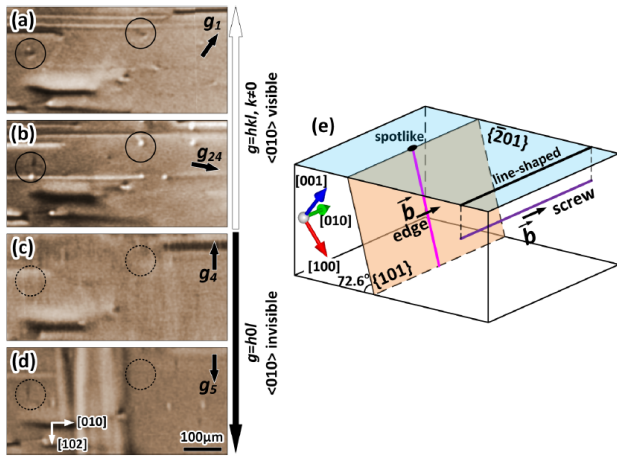


Fig. 3: Spotlike contrasts in the XRT images used to identify the Burgers vector $\vec{b} = \langle 010 \rangle_{\text{edge}}$, taken at the same \vec{g} -vectors as in Fig. 2 [2].

Fig. 3(a)–(d) show XRT images used to identify $\vec{b} = \langle 010 \rangle$ via spotlike contrasts. These images correspond to the areas indicated by the dotted rectangular frames in the upper-right corners of Fig. 2 (a)–(d). The \vec{g} vectors used here are the same as those used in Fig. 2. Two spotlike contrasts identified as edge-type $\vec{b} = \langle 010 \rangle$ dislocations are marked by circles. They have the same visibility as the line-shaped b -axis screw-type dislocations at the four \vec{g} vectors. The schematic drawing in Fig. 3(e) illustrates the line-shaped contrast caused by the screw-type $\vec{b} = \langle 010 \rangle$ dislocation that is present in the $\{201\}$ plane and a spotlike contrast caused by the edge-type $\vec{b} = \langle 010 \rangle$ dislocation that is present in the $\{101\}$ plane.

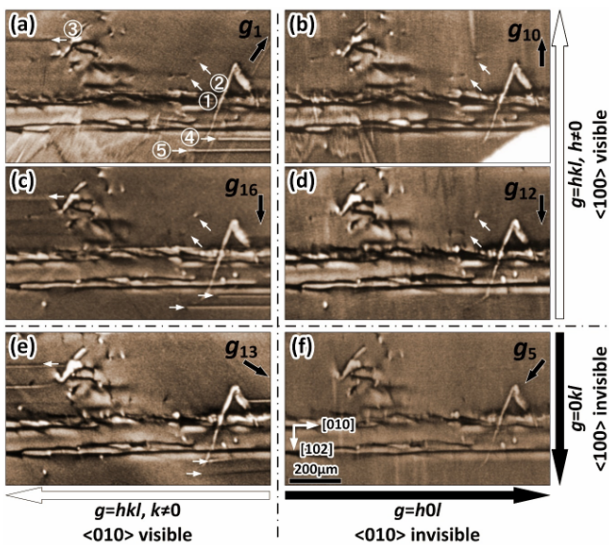


Fig. 4: XRT images used to identify Burgers vector $\vec{b} = \langle 100 \rangle$, taken at (a) $\vec{g}_1 = \bar{1}\bar{1}12$, (b) $\vec{g}_{10} = \bar{1}201$, (c) $\vec{g}_{16} = \bar{6}26$, (d) $\vec{g}_{12} = \bar{2}06$, (e) $\vec{g}_{13} = 0\bar{2}6$, and (f) $\vec{g}_5 = 006$ [2].

Another representative dislocation type is the one with $\vec{b} = \langle 100 \rangle$ because lattice a is the greatest one among the three axis. Identifying this type of dislocation requires \vec{g}_x and \vec{g}_y in the form of $\vec{g} = 0kl$. Here, we select $\vec{g}_x = \vec{g}_{13} = 0\bar{2}6$ and $\vec{g}_y = \vec{g}_5 = 006$ as the invisible conditions and $\vec{g}_1 = \bar{1}\bar{1}12$, $\vec{g}_{10} = \bar{1}201$, $\vec{g}_{16} = \bar{6}26$, and $\vec{g}_{12} = \bar{2}06$ as the visible conditions for $\vec{b} = \langle 100 \rangle$. Fig. 4 shows XRT images taken at the six \vec{g} vectors selected above. In this area, one can see two dislocations labeled 1 and 2 that satisfy the $\vec{g} \cdot \vec{b}$ invisibility criterion for $\vec{b} = \langle 100 \rangle$ dislocations, i.e., they are visible in Fig. 4(a)–(d) but not in Fig. 4(e) and (f). Although the Burgers vector of $\langle 100 \rangle$ is expected to give rise to a large strain field, the XRT spots from this type of dislocation do not exhibit a notable size difference when compared to other types. In Fig. 4, b -axis screw-type dislocations (the dislocations labeled 3, 4, and 5) are confirmed again by comparing more \vec{g} vectors than in Fig. 2. These dislocations are visible only in the three images on the left side, which have \vec{g} vectors in the form of $\vec{g} = hkl$, $k \neq 0$.

In this way, we identified a total of 12 types of Burgers vectors [2]. Some of these Burgers vectors, such as $\vec{b} = \langle 10\bar{1} \rangle$, $\frac{1}{2} \langle 132 \rangle$, $\frac{1}{2} \langle 1\bar{3}2 \rangle$, $\langle 001 \rangle$, and $\langle 100 \rangle$, were confirmed experimentally for the first time.

Acknowledgement

One of the authors Y.Y. is grateful to Dr. Y. Takahashi for her kind instructions on experimental operations.

References

- [1] H. Yamaguchi, A. Kuramata, and T. Masui, Superlattice Microst. **99**, 99 (2016)
- [2] Y. Yao, Y. Sugawara, and Y. Ishikawa, J. Appl. Phys. **127**, 205110 (2020).

* y_yao@jfcc.or.jp